

# Dalton Transactions

Accepted Manuscript



This is an *Accepted Manuscript*, which has been through the Royal Society of Chemistry peer review process and has been accepted for publication.

*Accepted Manuscripts* are published online shortly after acceptance, before technical editing, formatting and proof reading. Using this free service, authors can make their results available to the community, in citable form, before we publish the edited article. We will replace this *Accepted Manuscript* with the edited and formatted *Advance Article* as soon as it is available.

You can find more information about *Accepted Manuscripts* in the [Information for Authors](#).

Please note that technical editing may introduce minor changes to the text and/or graphics, which may alter content. The journal's standard [Terms & Conditions](#) and the [Ethical guidelines](#) still apply. In no event shall the Royal Society of Chemistry be held responsible for any errors or omissions in this *Accepted Manuscript* or any consequences arising from the use of any information it contains.



Cite this: DOI: 10.1039/xxxxxxxxxx

## Structural and magnetic properties of the low-dimensional fluoride $\beta\text{-FeF}_3(\text{H}_2\text{O})_2\cdot\text{H}_2\text{O}$

Gwilherm Nénert,<sup>\*a</sup> Oscar Fabelo,<sup>b</sup> Kerstin Forsberg,<sup>c</sup> Claire V. Colin,<sup>d,e</sup> and Juan Rodríguez-Carvajal,<sup>b</sup>

Received Date

Accepted Date

DOI: 10.1039/xxxxxxxxxx

www.rsc.org/journalname

We have reinvestigated the crystal structure of the low-dimensional fluoride  $\beta\text{-FeF}_3(\text{H}_2\text{O})_2\cdot\text{H}_2\text{O}$  using high resolution neutron and X-ray diffraction data. Moreover we have studied the magnetic behavior of this material combining medium resolution and high flux neutron powder diffraction together with magnetic susceptibility measurements. This fluoride compound exhibits vertex-shared 1D  $\text{Fe}^{3+}$  octahedral chains, which are extended along the *c*-axis. The magnetic interaction between adjacent chains involve super-superexchange interactions via an extensive network of hydrogen bonds. This interchain hydrogen bonding scheme is sufficiently strong to induce a long range magnetic order appearing below  $T_N = 20(1)$  K. The magnetic order is characterized by the propagation vector  $\mathbf{k} = (0, 0, \frac{1}{2})$ , giving rise to a strictly antiferromagnetic structure where the  $\text{Fe}^{3+}$  spins are lying within the *ab*-plane. Magnetic exchange couplings extracted from magnetization measurements are found to be  $J_{\parallel}/k_B = -18$  K and  $J_{\perp}/k_B = -3$  K. These values are in good agreement with the neutron diffraction data, which show that the system became antiferromagnetically ordered at ca.  $T_N = 20(1)$  K.

### 1 Introduction

Stimulated by the recent progress in synthesizing frustrated magnetic materials with strong quantum fluctuations and by the rich behavior of such magnetic systems, there is presently an enormous interest in frustrated quantum spin systems.<sup>1</sup> The frustration is generated by the competition of different kinds of interaction and/or by the lattice geometry. As a result, in the ground state all magnetic exchange interactions are not fully satisfied. The ground-state of frustrated spin systems is therefore highly degenerate and new induced symmetries give rise to spectacular and often unexpected behavior at finite temperatures. Many properties of frustrated systems are still not well understood at present. One of the main reasons is that these systems usually present not only low dimensional properties but also magnetic frustration such as  $\text{LiCuVO}_4$ ,  $\text{A}_2\text{CuO}_2$  ( $A = \text{Li}, \text{Na}$ ) and  $\text{ACu}_2\text{O}_2$  ( $A = \text{Li}, \text{Na}$ ).<sup>2</sup> Consequently, it is difficult to disentangle between the two aspects described above in order to determine which parameter plays the most important role in defining the magnetic

ground state. This is particularly important when it comes to the understanding the origin of multiferroicity in these materials.<sup>3–6</sup>

While a lot of work is dedicated to oxides, fluorides have been shown to be an excellent playground for investigating low dimensional magnetism and multiferroic materials.<sup>7</sup> Low dimensional spin systems stand for a promising subject in solid-state physics due to the possibility to observe numerous quantum phenomena. In contrast to magnetic systems with classical long-ranged ferromagnetic or antiferromagnetic order, the interplay of low dimension, competing interactions and strong quantum fluctuations, as well as unusual spin and charge correlations, gives rise to a wealth of fascinating phenomena. Furthermore, transition metal fluorides have recently emerged as a promising new family of lithium ion battery cathode materials. Especially iron(III) fluorides have attracted attention due to their high theoretical capacity and low cost.<sup>8</sup> Further, the  $\alpha$ -phase of  $\text{FeF}_3\cdot 3\text{H}_2\text{O}$  can be used to synthesize semiconducting hematite nanowires for photoelectrochemical applications.<sup>9</sup> For all these reasons, additional work is required to investigate in more details the structural and magnetic properties of transition metal fluorides.

In this contribution, we have investigated the low-dimensional fluoride  $\beta\text{-FeF}_3(\text{H}_2\text{O})_2\cdot\text{H}_2\text{O}$  related to the rosenbergite mineral.<sup>10</sup>  $\text{MF}_3\cdot 3\text{H}_2\text{O}$  ( $M = \text{V}, \text{Cr}, \text{Mn}, \text{Fe}, \text{Al}, \text{Ga}$  or  $\text{In}$ ) fluorides crystallize in two possible crystal structures.<sup>11,12</sup> The  $\alpha$ -phase exhibits the symmetry  $R\bar{3}m$  ( $a \approx 9.3$  Å and  $c \approx 4.6$  Å) and is characterized by isolated  $\text{MF}_3(\text{H}_2\text{O})_3$  octahedra, where the  $\text{H}_2\text{O}$  molecules

<sup>a</sup> PANalytical B. V., Lelyweg 1, 7602 EA Almelo, The Netherlands; E-mail: gwilherm.nenert@panalytical.com

<sup>b</sup> Institut Laue-Langevin, Diffraction Group, 71 Avenue des Martyrs, 38000 Grenoble, France.

<sup>c</sup> School of Chemical Science and Engineering, Royal Institute of Technology, Teknikringen 42, SE 100 44 Stockholm, Sweden.

<sup>d</sup> Université Grenoble Alpes, Institut Néel, F-38042 Grenoble, France

<sup>e</sup> CNRS, Institut Néel, F-38042 Grenoble, France

Atom	Wyckoff	x	y	z	$U_{iso}$	Occ.
Fe	2c	$\frac{1}{4}$	$\frac{1}{4}$	0.8519(3)	0.0200(6)	1.0
F(1)	2c	$\frac{1}{4}$	$\frac{1}{4}$	0.3527(8)	0.0350(12)	1.0
O(1 <sub>w</sub> )	2b	$\frac{1}{4}$	$\frac{3}{4}$	$\frac{1}{2}$	0.0215(11)	1.0
O(1)	8g	0.85273(20)	0.9769(2)	0.1413(6)	0.0297(10)	0.5
F(2)	8g	0.85273(20)	0.9769(2)	0.1413(6)	0.0297(10)	0.5
H(1 <sub>w</sub> )	8g	0.1777(10)	0.9204(9)	0.729(2)	0.0428(19)	0.5
H(1)	8g	0.3481(8)	0.7840(8)	0.360(2)	0.0470(17)	0.5
H(2)	8g	0.0315(11)	-0.0028(13)	-0.040(3)	0.0463(20)	0.5

**Table 1** Crystallographic coordinates of  $\beta$ -FeF<sub>3</sub>(H<sub>2</sub>O)<sub>2</sub>·H<sub>2</sub>O extracted from the multipattern Rietveld refinement carried out using neutron (D20) and high resolution X-ray (K $\alpha_1$  Cobalt radiation) diffraction data using the space group  $P4/n$  (#85) at room temperature. Cell parameters:  $a = 7.83965(13)$  Å and  $c = 3.87551(6)$  Å.

Atom	$U_{11}$	$U_{22}$	$U_{33}$	$U_{12}$	$U_{13}$	$U_{23}$
Fe	0.0208(5)	0.0208(5)	0.0184(7)	0(-)	0(-)	0(-)
F(1)	0.0500(11)	0.0500(11)	0.0049(13)	0(-)	0(-)	0(-)
O(1 <sub>w</sub> )	0.0199(9)	0.0199(9)	0.0247(14)	0(-)	0(-)	0(-)
F(2)/O(1)	0.0288(9)	0.0168(9)	0.0435(10)	-0.0072(7)	0.0143(11)	-0.0045(9)

**Table 2** Anisotropic atomic displacement parameters  $U_{ij}$  (in units of Å<sup>2</sup>) of  $\beta$ -FeF<sub>3</sub>(H<sub>2</sub>O)<sub>2</sub>·H<sub>2</sub>O at room temperature. The parameters were obtained through the multipattern refinement of neutron and X-ray data.

and F<sup>-</sup> ions are sharing same crystallographic positions. The  $\beta$ -phase crystallizes in the space group  $P4/n$  ( $a \approx 7.8$  Å and  $c \approx 3.9$  Å). The  $\beta$ -phase is characterized by 1D linear chains of vertex sharing octahedra running along the tetragonal  $c$ -axis. The mineral rosenbergite (composition AlF<sub>3</sub>(H<sub>2</sub>O)<sub>3</sub>) crystallizes in the  $\beta$  phase and its structural formula is AlF[F $\frac{1}{2}$ (H<sub>2</sub>O) $\frac{1}{2}$ ]<sub>4</sub>·4H<sub>2</sub>O.<sup>10</sup> While several compositions have been suggested to crystallize in the two different polymorphs, however the previously reported work does not provide a precise structural characterization mainly due to the disorder between F<sup>-</sup> and H<sub>2</sub>O molecules. Moreover, the stability of the two different polymorph plays an important role in these compounds. The  $\beta$ -phase tends to be the most thermodynamically stable as illustrated by the case of MF<sub>3</sub>(H<sub>2</sub>O)<sub>3</sub> (M = Al, Fe) where the  $\alpha$ -phase transforms to the  $\beta$ -phase as function of time over a period of one year.<sup>12,13</sup>

The magnetic susceptibility measurement on the title compound presents some low dimensional antiferromagnetic character at high temperature and shows three dimensional magnetic order at low temperature (ca. 20 K), however the magnetic and precise nuclear structures were unknown as well as the mechanism producing the ordered state.

## 2 Experiment

$\beta$ -FeF<sub>3</sub>(H<sub>2</sub>O)<sub>2</sub>·H<sub>2</sub>O was prepared by evaporation from an HF solution at 55°C. First ferric hydroxide was precipitated from an iron nitrate solution at room temperature, prepared from Fe(NO<sub>3</sub>)<sub>3</sub>·9H<sub>2</sub>O (PA), by drop wise addition of 25% ammonia solution (PA) under vigorous stirring. The precipitate was vacuum filtered and repeatedly washed with de-ionized water. The freshly precipitated ferric hydroxide was dissolved in 20% hydrofluoric acid in HDPE wide-mouth bottles placed in a thermostatic water bath held at 55°C. Then the solution was concentrated by evaporation at 55°C  $\pm$  0.01°C during continuous stirring. The very

light pink precipitate was vacuum filtered and washed with water at 60°C and then with ethanol. The crystal sample was then dried at 60°C for 50h.

Neutron powder diffraction data were collected on the high counting efficiency diffractometer D20 working in high resolution mode at the Institut Laue Langevin. The measurements were carried out at room temperature using a vacuum chamber in order to reduce the incoherent air scattering. The pattern was collected in the  $2\theta$ -range from 0° to 151° with a step size  $\Delta 2\theta = 0.1^\circ$ . The neutrons were monochromated using the (117) Bragg reflexion of a germanium (Ge) monochromator with a take-off angle of 120° corresponding to a nominal wavelength of 1.35 Å.<sup>14</sup> The exact determination of the wavelength ( $\lambda_{neutron} = 1.35845(5)$  Å) was performed by constraining the cell parameters to those previously obtained under the same conditions using high resolution X-ray powder diffraction data.

In order to determine the magnetic structure, additional neutron powder diffraction data at low temperature (from 1.8 to 20 K) were collected on the double axis multicounter high-flux and medium resolution D1B diffractometer operated with a wavelength of 2.52 Å, obtained from a vertical focusing pyrolytic graphite monochromator. The diffractometer was operated with a Helium Vanadium tail cryostat (Orange Cryostat). The detection is made via a position sensitive detector covering the angular range from 0.7 - 128.7°.

High-resolution X-ray powder diffraction data for  $\beta$ -FeF<sub>3</sub>(H<sub>2</sub>O)<sub>2</sub>·H<sub>2</sub>O were collected on a PANalytical diffractometer using monochromatic cobalt K $\alpha_1$  radiation using an incident beam Johansson Ge monochromator. We used fixed 0.25° divergence slit with primary and secondary side 0.02 rad Soller slits. In order to improve the data quality, variable counting time was used resulting in three different X-ray patterns. The first pattern was collected in the  $2\theta$  range 16-145°, the second

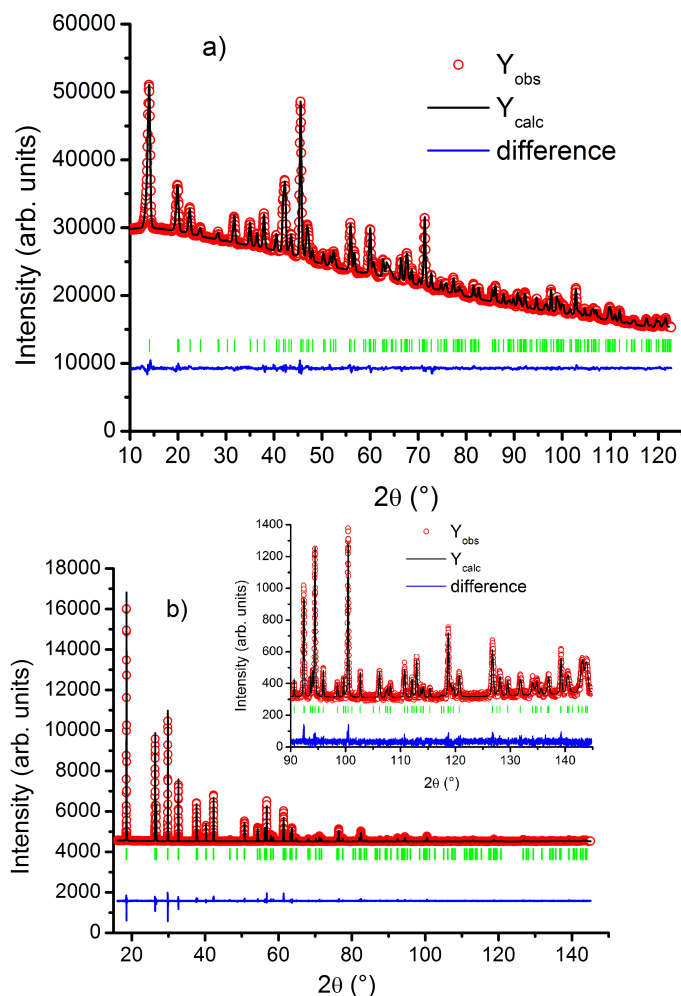


**Fig. 1** Combined Rietveld refinement of  $\beta$ - $\text{FeF}_3(\text{H}_2\text{O})_2 \cdot \text{H}_2\text{O}$  at room temperature using a) neutron data measured on D20 (Statistics:  $R_F = 1.00$ ,  $R_{\text{Bragg}} = 2.04$ ), b) high resolution  $\text{K}\alpha_1$  X-ray on a PANalytical diffractometer (Statistics:  $R_F = 4.10$ ,  $R_{\text{Bragg}} = 4.54$ ) and high resolution  $\text{K}\alpha_1$  X-ray on a PANalytical diffractometer for the high angle part (Statistics:  $R_F = 3.77$ ,  $R_{\text{Bragg}} = 6.86$ ) in the inset.

from 50 to 90° and the last one from 90 to 145° with increasing counting time.

Polycrystalline  $\beta$ - $\text{FeF}_3(\text{H}_2\text{O})_2 \cdot \text{H}_2\text{O}$  magnetization measurements were carried out with a Quantum Design SQUID magnetometer in the temperature range of 2-350 K and external magnetic fields up to 5 T.

### 3 Results and discussion

#### 3.1 Crystal structure

In order to investigate in details the crystal structure of  $\beta$ - $\text{FeF}_3(\text{H}_2\text{O})_2 \cdot \text{H}_2\text{O}$ , we have performed a combined Rietveld refinement using high resolution monochromatic cobalt  $\text{K}\alpha_1$  X-ray and neutron powder diffraction data using the multipattern option in the FullProf program suite.<sup>15</sup> The neutron data allow unambiguously to determine the position of the hydrogen atoms, which have a negligible scattering power using X-ray. The initial structural model including the hydrogen atoms were obtained by the simulated annealing protocol. The fit of the high resolution neu-

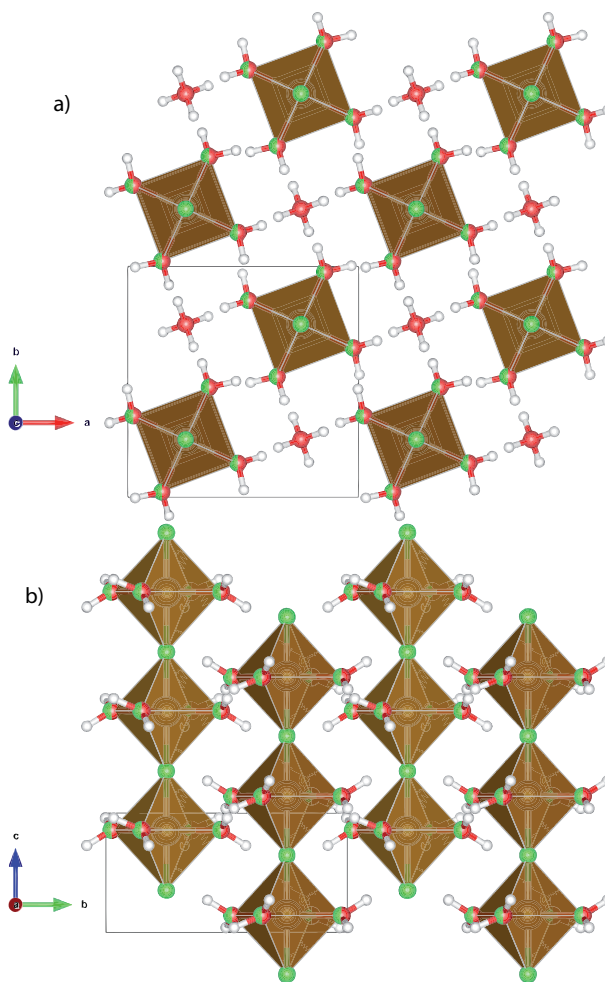


**Fig. 2** Crystal structure of  $\beta$ - $\text{FeF}_3(\text{H}_2\text{O})_2 \cdot \text{H}_2\text{O}$  represented a) in the  $ab$ -plane and b) projected along the  $a$ -axis. In the projection along the  $c$ -axis, the crystallization water molecule have been omitted for clarity.

tron data collected at room temperature gives rise to a structural model with an accurate description of the H-bond network which resembles the rosenbergite structure.

The use of multipattern refinement combining the neutron diffraction with the three variable counting time for X-ray pattern enables us to refine precisely the crystal structure of  $\beta$ - $\text{FeF}_3(\text{H}_2\text{O})_2 \cdot \text{H}_2\text{O}$  including the anisotropic thermal parameters of the atoms (besides the hydrogen atoms). We present in Figure 1 the fit and the goodness of fit of the room temperature data using the multipattern approach. The Table 1 shows the crystallographic details and the resulting atomic coordinates obtained from the final multipattern Rietveld analysis.

The crystal structure of the  $\beta$ - $\text{FeF}_3(\text{H}_2\text{O})_2 \cdot \text{H}_2\text{O}$  compound, is built up from  $\text{Fe}[\text{F}_4(\text{H}_2\text{O})_2]$  octahedra which are connected, sharing a vertex, along the tetragonal  $c$ -axis, giving rise to one dimensional (1D) chains. The Fe ions are occupying the  $2c$  Wyckoff position, which lies on a four-fold rotation axis along the tetragonal  $c$ -axis. The shared vertex of the octahedra, the apical position, is occupied by the F(1) atom, while the other four remaining positions, that complete the equatorial plane, are filled by F(2) and

O(1). Different structural models were tested, however the only model that refines successfully the data involves a shared occupancy of 50% between F(2) and O(1) which lie on the 8g Wyckoff position. It should be noted that the bond distance in the apical position are slightly shorter than those of the equatorial plane, this effect is in agreement with the larger electro-negativity of F<sup>-</sup> ion with respect to the water molecule. The hydrogen atoms of the coordination water molecules have been located in general position and refined with 50% of occupancy.

The crystallization water molecules are located in the empty space between chains, the oxygen atom of these crystallization water molecules [O(1<sub>w</sub>)] are placed on the 2b Wyckoff position, which lies on a four-fold rotoinversion axis along the tetragonal c-axis, and refined with a full occupancy. However, the hydrogen atoms of the crystallization water molecule [H(1<sub>w</sub>)] were refined with a occupancy of 50%, due to the application of the four-fold rotoinversion axis. This disordered model, can be seen as the superposition of six different crystallization water conformation along the crystal. The O-H bond distance is 0.978(7) Å and the angle H(1<sub>w</sub>)-O(1<sub>w</sub>)-H(1<sub>w</sub>) is 107.9(4)°. This is in good agreement with values reported in other water containing mineral.<sup>16</sup>

The extensive network of H-bonds involves both crystallization and coordination water molecules as donor, and crystallization water molecules and F<sup>-</sup> ions as acceptors. The H-bond distances between crystallization water molecules and F<sup>-</sup> ions have a O(1<sub>w</sub>)...F(2) bond distance of 2.677(2) Å and a H(1)...F(2) bond distance of 1.700(7) Å and an angle between O(1<sub>w</sub>)-H(1<sub>w</sub>)...F(2) of 175.7(5)°. The H-bond through coordination and crystallization water molecules have a O(1<sub>w</sub>)...O(1) bond distance of 2.677(2) Å and a H(1<sub>w</sub>)...O(1<sub>w</sub>) bond distance of 1.701(8) Å and an angle between O(1)-H(1<sub>w</sub>)...O(1<sub>w</sub>) of 174.4(5)°, values which are very similar to the O(1<sub>w</sub>)-H(1<sub>w</sub>)...F(2) H-bond.

The H-bonds involving coordination water molecules and F<sup>-</sup> ions present a slightly shorter bond distances. The partial presence of F<sup>-</sup> ions in both sites could be the reason for the short hydrogen bonds with values of O(1)...F(2) of 2.582(3) Å and a H(2)...F(2) bond distance of 1.58(1) Å and an angle between O(1)-H(2)...F(2) of 173.4(5)°. This H...O bond distance is slightly shorter than those previously observed in other minerals such as brazilianite.<sup>17</sup> The short bond distances present in the title compound give rise to a non-negligible exchange coupling pathway between the 1D chains. These interactions must be taken into account in order to understand the long range magnetic order at low temperatures.

### 3.2 Magnetic properties

The crystal structure of β-FeF<sub>3</sub>(H<sub>2</sub>O)<sub>2</sub>·H<sub>2</sub>O exhibits one dimensional chains running along the c-axis. Those chains are only coupled by hydrogen bonding and thus one would expect some one dimensional magnetism. Temperature and magnetic field dependence of the magnetic susceptibility have been investigated in the temperature range 2 K to 350 K. The temperature dependence of the zero field cooled susceptibility measured in an applied magnetic field of 1000 Oe is shown in Figure 3. The mag-

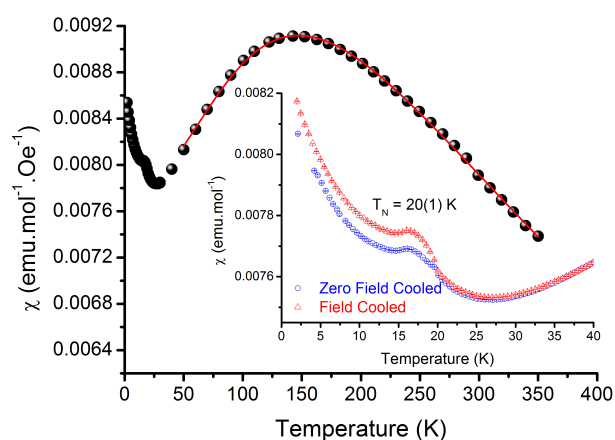


**Fig. 3** (Color online) Zero-field-cooled magnetic susceptibility of β-FeF<sub>3</sub>(H<sub>2</sub>O)<sub>2</sub>·H<sub>2</sub>O as function of temperature recorded with an applied magnetic field of 1000 Oe. The solid line represents the fit of the data between 50 and 350 K using equation (3). In the insert, we show the magnetic susceptibility data measured in zero field-cooled (ZFC) and field-cooled (FC) with an applied magnetic field of 100 Oe.

netic susceptibility of β-FeF<sub>3</sub>(H<sub>2</sub>O)<sub>2</sub>·H<sub>2</sub>O clearly exhibits a very broad maximum centered around 150 K. This broad maximum is characteristic of low dimensional magnetism as expected from the crystal structure.<sup>18</sup> At low temperature an additional signal is visible, this second anomaly suggests the occurrence of long range magnetic order. The magnetic susceptibility at high temperature (from 270 to 350 K) was analyzed through the Curie-Weiss formula  $\chi = \frac{C}{T-\theta}$ , showing a negative Weiss constant ( $\theta$ ) of -232 K, suggesting the occurrence of antiferromagnetic interactions.

The low temperature region from 2 K to 40 K was more accurately studied by measuring the magnetic susceptibility under an external applied field of 100 Oe after a field-cooled (FC) and zero-field-cooled (ZFC) preparation. These additional data are presented as an insert in Figure 3. The splitting observed at ca. 20 K suggests the occurrence of some long range magnetic order. The antiferromagnetic behavior at low temperature has been confirmed through the magnetization as a function of the magnetic field at 2 K see Figure 4. The magnetization curve presents a slight sigmoidal shape with a change of curvature at 8000 Oe, this metamagnetic behavior suggests the overcome of some of the antiferromagnetic interactions, however the antiferromagnetic interactions remain dominant. The Néel temperature obtained from FC-ZFC measurements, is in good agreement with the magnetic ordering determined from previous Mössbauer data.<sup>19</sup>

Based on the crystal structure, the magnetic behavior can be interpreted based on isolated chains. For half-integer  $S = \frac{5}{2}$  chains, the broad maximum in  $\chi(T)$  is related to the intrachain exchange interaction parameter  $|J_{\parallel}|$  through the formula<sup>20</sup>

$$T_M \simeq 10.6 |J_{\parallel}| \quad (1)$$

To estimate the averaged interchain exchange interaction parameter  $|J_{\perp}|$ , the Schultz formula<sup>21</sup> can be used

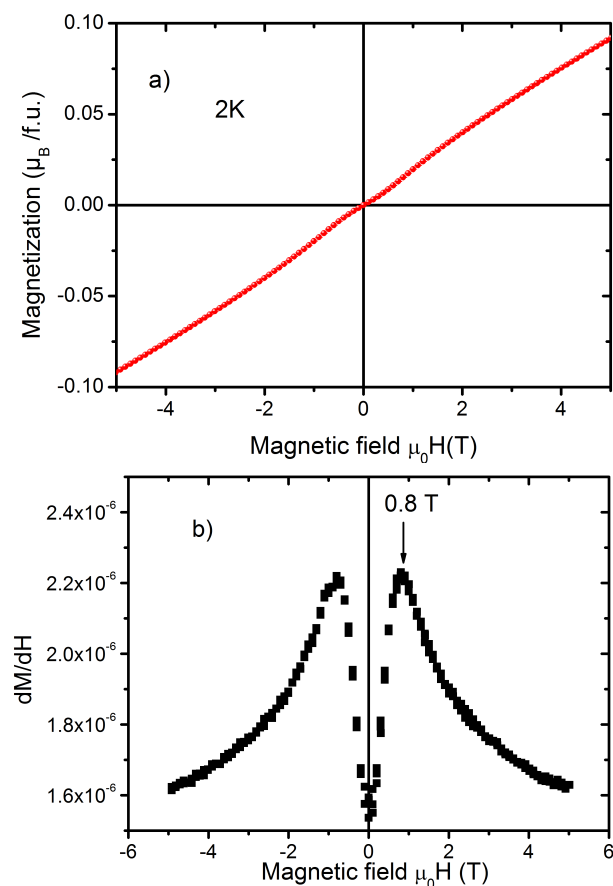


**Fig. 4** (Color Online) a) Magnetic field dependence of the magnetic susceptibility of  $\beta\text{-FeF}_3(\text{H}_2\text{O})_2\cdot\text{H}_2\text{O}$  as function of temperature and magnetic field; b) Derivative of the magnetic field dependence of the magnetic susceptibility demonstrating the existence of a weak metamagnetic behavior.

$$|J_{\perp}| = \frac{T_N}{1.28n\sqrt{\ln\frac{5.8|J_{\parallel}}{T_N}}} \quad (2)$$

Here  $n = 4$  is the coordination number for interchain interactions in  $\beta\text{-FeF}_3(\text{H}_2\text{O})_2\cdot\text{H}_2\text{O}$ . Using equations 1 and 2, one obtain an estimate of  $|J_{\parallel}| \simeq 14$  K and  $|J_{\perp}| \simeq 3.3$  K. These results suggest that the interchain coupling is significant, which explains the existence of a long range magnetic order at low temperature. However, eqs. (1) and (2) do not give any indication about the sign of the magnetic interactions. The Weiss temperature suggests strong antiferromagnetic interactions and thus  $J_{\parallel}$  is expected to be negative. This is also in agreement with the Goodenough-Kanamori-Anderson rules for nearly  $180^\circ$  Fe-F(1)-Fe super-exchange interactions.<sup>22</sup> In order to confirm, the value of the interchain coupling  $J_{\parallel}$  and confirm its sign, we have treated the magnetic susceptibility data using low dimensional magnetism formula.<sup>20</sup>

Based on the spin-spin Hamiltonian  $\mathcal{H} = -J_{\parallel}\sum_i \mathbf{S}_i\mathbf{S}_{i+1}$ , where  $J_{\parallel}$  is the intrachain exchange coupling [the magnetic interaction between  $\text{Fe}^{3+}$  ions through the F(1) bridge along the  $c$ -axis], the magnetic susceptibility can be expressed through the Fisher approach for uniform chain of classical spins as:<sup>23</sup>

$$\chi_{\text{chain}} = \frac{Ng^2\beta^2S(S+1)}{3k_bT} \times \frac{1+u}{1-u} \quad (3)$$

where  $u$  is the well-known Langevin function defined as:

$$u = \coth\left[\frac{J_{\parallel}S(S+1)}{k_bT}\right] - \frac{k_bT}{J_{\parallel}S(S+1)} \quad (4)$$

the  $N$ ,  $g$  and  $k_b$  constants have their usual meaning and  $S = \frac{5}{2}$  for  $\text{Fe}^{3+}$  ions. The resulting fit of the data in the temperature range 50 - 350 K is shown in Figure 3. The extracted value for  $J_{\parallel}$  is -18 K with a  $g$  value of 2.14. Although relatively large, this  $g$  value is not uncommon for low dimensional system, see for instance Ref<sup>24</sup>. This result confirms the order of magnitude of the magnetic interactions within the chains and its antiferromagnetic nature. The associated  $|J_{\perp}|$  determined using Eq. (1) is 3 K.

In the mean field approximation, the paramagnetic Curie-Weiss temperature  $\theta$  is given by:<sup>18</sup>

$$\theta = \frac{S(S+1)}{3k_b} \sum_{i=1}^n z_i J_i \quad (5)$$

where  $S = \frac{5}{2}$  for the spin  $\text{Fe}^{3+}$ ,  $J_i$  are the different exchange integrals between magnetic sites, and  $z_i$  is the number of nearest-neighbor magnetic sites around the magnetic site  $i$ . As an additional consistency check of the determination of  $J_{\parallel}$  and  $J_{\perp}$  determined using Eqs. (2) and (3), we compared the paramagnetic Curie temperature  $\theta$  obtained from the Curie-Weiss fit with the value derived using the values  $J_{\parallel}$  and  $J_{\perp}$  and Eq. (5).

$$\chi = \frac{C}{T-\theta} = \frac{C}{T-(\theta_{\parallel} + \theta_{\perp})} \quad (6)$$

With  $z_{\parallel} = 2$ ,  $z_{\perp} = 4$ ,  $J_{\parallel}/k_b = -18$  K and  $J_{\perp}/k_b = -3$  K (assuming antiferromagnetic coupling between the chains);  $\theta$  is calculated to be -224 K according to Eq. (5). This is in good agreement with the value of -232 K deduced from the fit of the high temperature susceptibility.

### 3.3 Magnetic structure

The temperature dependence of the neutron powder diffraction patterns were collected as function of temperature on the D1B diffractometer. Below about 20 K, new diffraction peaks appear. This confirms the appearance of a magnetic ordering below  $T = 20$  K, in good agreement with the magnetic susceptibility. The indexing of the observed magnetic reflections in the lowest temperature pattern was done using the k-Search program included in the FullProf suite.<sup>25</sup> The only solution which indexes the observed magnetic reflections is the  $\mathbf{k} = (0, 0, \frac{1}{2})$  propagation vector.

The possible magnetic structures compatible with the symmetry of  $\beta\text{-FeF}_3(\text{H}_2\text{O})_2\cdot\text{H}_2\text{O}$  were determined through the representational analysis technique described by Bertaut,<sup>26</sup> using the BasReps program included in the Fullprof suite.<sup>27</sup> The magnetic moment of an atom  $j$  in the unit cell  $l$  is, in general, given by

	1 000	2 <sub>00z</sub>   $\frac{1}{2}\frac{1}{2}0$	4 <sub>00z</sub> <sup>+</sup>   $\frac{1}{2}00$	4 <sub>00z</sub> <sup>-</sup>   $0\frac{1}{2}0$	-1 000	m <sub>xy0</sub>   $\frac{1}{2}\frac{1}{2}0$	-4 <sub>00z</sub> <sup>+</sup>   $\frac{1}{2}00$	-4 <sub>00z</sub> <sup>-</sup>   $0\frac{1}{2}0$
Γ <sub>1</sub>	1	1	1	1	1	1	1	1
Γ <sub>2</sub>	1	1	-1	-1	1	1	-1	-1
Γ <sub>3</sub>	$\begin{pmatrix} 1 & 0 \\ 0 & 1 \end{pmatrix}$	$\begin{pmatrix} -1 & 0 \\ 0 & -1 \end{pmatrix}$	$\begin{pmatrix} 0 & 1 \\ -1 & 0 \end{pmatrix}$	$\begin{pmatrix} 0 & -1 \\ 1 & 0 \end{pmatrix}$	$\begin{pmatrix} 1 & 0 \\ 0 & 1 \end{pmatrix}$	$\begin{pmatrix} -1 & 0 \\ 0 & -1 \end{pmatrix}$	$\begin{pmatrix} 0 & 1 \\ -1 & 0 \end{pmatrix}$	$\begin{pmatrix} 0 & -1 \\ 1 & 0 \end{pmatrix}$
Γ <sub>4</sub>	1	1	1	1	-1	-1	-1	-1
Γ <sub>5</sub>	1	1	-1	-1	-1	-1	1	1
Γ <sub>6</sub>	$\begin{pmatrix} 1 & 0 \\ 0 & 1 \end{pmatrix}$	$\begin{pmatrix} -1 & 0 \\ 0 & -1 \end{pmatrix}$	$\begin{pmatrix} 0 & 1 \\ -1 & 0 \end{pmatrix}$	$\begin{pmatrix} 0 & -1 \\ 1 & 0 \end{pmatrix}$	$\begin{pmatrix} -1 & 0 \\ 0 & -1 \end{pmatrix}$	$\begin{pmatrix} 1 & 0 \\ 0 & 1 \end{pmatrix}$	$\begin{pmatrix} 0 & 1 \\ -1 & 0 \end{pmatrix}$	$\begin{pmatrix} 0 & -1 \\ 1 & 0 \end{pmatrix}$

**Table 3** Physically irreducible representations of the space group  $P4/n$  for  $\mathbf{k} = (0, 0, \frac{1}{2})$ . The symmetry elements are written according to Seitz's notation.

<i>p-irreps/Symmetry</i>	<i>x, y, z</i>	<i>-x, -y, -z</i>
Γ <sub>1</sub>	(001)	(00-1)
Γ <sub>3</sub>	(100) (010)	(-100) (0-10)
Γ <sub>4</sub>	(001)	(001)
Γ <sub>6</sub>	(100) (010)	(100) (010)

**Table 4** Basis vectors of the four possible physically irreducible representations for the Fe<sup>3+</sup>(2c) atoms

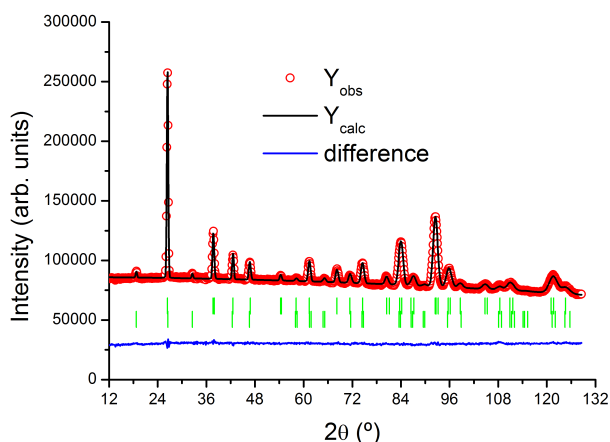


**Fig. 5** Rietveld refinement of the data recorded on D1B at 1.8 K using the magnetic structure model given by the magnetic space group  $P_b2_1/c$  in BNS notation. Cell parameters at 1.8 K:  $a = 7.80949(9)$  Å and  $c = 3.87669(7)$ . Statistics:  $R_F = 1.6$ ,  $R_{Bragg} = 2.27$ .

the Fourier series:  $\mathbf{m}_{jl} = \sum_{\mathbf{k}} \mathbf{S}_{\mathbf{k}j} \exp(-2\pi i \mathbf{k} \cdot \mathbf{R}_l)$ . The representational analysis provides the expression of the vector Fourier coefficients  $\mathbf{S}_{\mathbf{k}j}$  as linear combinations of basis functions of the irreducible representations (*irreps*) of the propagation vector group  $G_{\mathbf{k}}$  formed by the subgroup of the space group  $G$  leaving invariant the propagation vector  $\mathbf{k}$ . The basis vectors describe the possible arrangements of magnetic structures.

BasReps program is able to work with *irreps* as well as with physically irreducible representations (*p-irreps*), the *p-irreps* are formed from the direct sum of two complex *irreps*, therefore the resulting matrices are equivalent to a set of real matrices.<sup>28</sup> In the present case, with structural space group  $P4/n$ , the  $\mathbf{k} = (0, 0, \frac{1}{2})$  propagation vector we have  $G_{\mathbf{k}} = P4/n$ , so the *irreps* of the group  $G_{\mathbf{k}}$ , we obtain eight one-dimensional *irreps*. In this case the Fourier series describing possible magnetic structures contain a single term so the Fourier coefficients  $\mathbf{S}_{\mathbf{k}j}$  should be real vectors equal to the magnetic moment of the atoms in the primitive cell

$\mathbf{S}_{\mathbf{k}j} = \mathbf{m}_j$ . The magnetic representation  $\Gamma_M$  for the Wyckoff position 2c can be decomposed as a direct sum of *irreps* by applying the great orthogonality theorem. From the six possible *irreps* for site 2c, only two are real, however neither of these solutions are able to reproduce the experimental data.

A survey of the imaginary representations shows that there are two pairs of complex conjugated *irreps*, and therefore they can be combined into two two-dimensional *p-irreps*. The *p-irreps* for  $G_{\mathbf{k}} = P4/n$  are displayed in Table 3.

The magnetic representation  $\Gamma_M$  for the Wyckoff position 2c can be decomposed as a direct sum of *p-irreps* using BasRep program, the *p-irreps* are read from the physically irreducible representations database created by Harold T. Stokes and Branton J. Campbell.<sup>29</sup> The *p-irreps* appear one time for  $\Gamma_1$  and  $\Gamma_4$  and two times for  $\Gamma_3$  and  $\Gamma_6$  (see Eq. 7).

$$\Gamma_M = \Gamma_1 \oplus 2\Gamma_3 \oplus \Gamma_4 \oplus 2\Gamma_6 \quad (7)$$

The magnetic moments for Fe<sup>3+</sup> site (2c Wyckoff position) are obtained from the basis vectors as  $\mathbf{m}_{2c}(1) = (0, 0, u)$  and  $\mathbf{m}_{2c}(2) = (0, 0, -u)$  for *p-irreps*  $\Gamma_1$  and  $\mathbf{m}_{2c}(1) = (0, 0, u)$  and  $\mathbf{m}_{2c}(2) = (0, 0, u)$  for *p-irreps*  $\Gamma_4$  (see Table 4), which correspond to a magnetic structure where the magnetic moment are aligned strictly along the *c*-axis. While for  $\Gamma_3$  and  $\Gamma_6$  the magnetic moments are given by  $\mathbf{m}_{2c}(1) = (u, v, 0)$  and  $\mathbf{m}_{2c}(2) = (-u, -v, 0)$  and by  $\mathbf{m}_{2c}(1) = (u, v, 0)$  and  $\mathbf{m}_{2c}(2) = (u, v, 0)$ , respectively. In both cases there are two degrees of freedom for the magnetic structure, which is symmetry constrained to be in the *ab*-plane. The Rietveld refinement of the low temperature pattern suggests that the magnetic structure is described only with the *p-irrep*  $\Gamma_3$ . The magnetic space group is  $P_c112_1/n$  in the non-standard setting  $\{\mathbf{a}, \mathbf{b}, 2\mathbf{c}; 0, 0, 0\}$ , while the magnetic space group in the standard setting is  $P_b2_1/c$  applying the further cell transformation  $\{\mathbf{a}, -\mathbf{c}, \mathbf{a}+\mathbf{b}; 0, 0, 1/4\}$ . The magnetic space group in the OG-notation corresponds to the  $P_{2b}2'/c$  symbol.<sup>30</sup>

However, from powder data, we are not able to distinguish

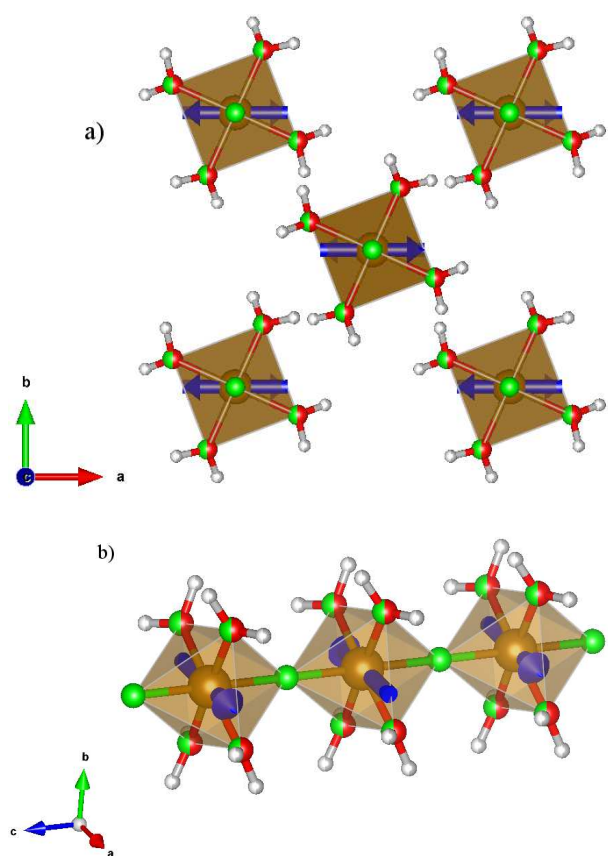


**Fig. 6** (Color online) Magnetic structure of  $\beta$ - $\text{FeF}_3(\text{H}_2\text{O})_2 \cdot \text{H}_2\text{O}$  a) projected along the  $c$ -axis and b) showing the coupling within the chains. The crystallization water molecules have been omitted for clarity.

within the  $ab$ -plane the direction of the magnetic moments. Therefore, in order to converge to one particular solution, we have considered that the magnetic moment is along the  $a$ -axis. Whatever direction of the magnetic moment is within the  $ab$ -plane, it gives the same calculated diffraction pattern. The resulting magnetic moment for the  $\text{Fe}^{3+}$  ions is  $3.23(4) \mu_B$ . This value is well below the spin-only value of  $5 \mu_B$ . This reduction about ca. 33% can be due to the spin delocalization from the  $\text{Fe}^{3+}$  ions to the coordinated  $\text{F}^-$  ions and/or O atoms or due to the low-dimensional character of this system, which gives rise to a significant reduction in the magnetic moment. Moreover similar reduction has been observed in other low dimensional systems.<sup>31</sup> In particular the  $\text{Rb}_2\text{MnF}_5$  low dimensional fluoride exhibits a reduction of the magnetic moment of ca. 18% [ $\mu(\text{Mn}^{3+}) = 3.3(1) \mu_B$ ].<sup>32</sup> The large diminution observed in the present compound suggests that both mechanisms are involved. The final fit of the powder diffraction data at 1.8 K is presented in Fig. 5.

The proposed magnetic structure can be explained by a simple consideration using a model based on three different isotropic exchange. The magnetic exchange couplings are mediated by super- or super-super-exchange interactions involving  $\text{Fe-F(1)-Fe}$ ,  $\text{Fe-O(1)-O(1)-Fe}$  and  $\text{Fe-F(1)-O(1)-Fe}$  exchange pathways with distances between the  $\text{Fe}^{3+}$  ions, ranged from ca. 3.87 to 6.17 Å. The  $\text{Fe-F(1)-Fe}$  super-exchange coupling correspond to the mag-

netic interactions along the  $c$ -axis ( $J_1$ ). The super-super exchange interactions can be divided in two different pathways through coordination water molecules  $\text{Fe-O(1)-O(1)-Fe}$  ( $J_2$ ) and through fluorine and crystallization water molecules  $\text{Fe-F(1)-O(1}_w\text{)-Fe}$  ( $J_3$ ), a topological view of the exchange coupling interactions can be seen in Figure 7. The value of the  $J_1$  interaction including the sign have been determined from the fit of the temperature evolution of the susceptibility. The global interchain interaction has been characterized as antiferromagnetic, based on the magnetization measurements. However, we are not able to obtain separately the values of  $J_2$  and  $J_3$ .

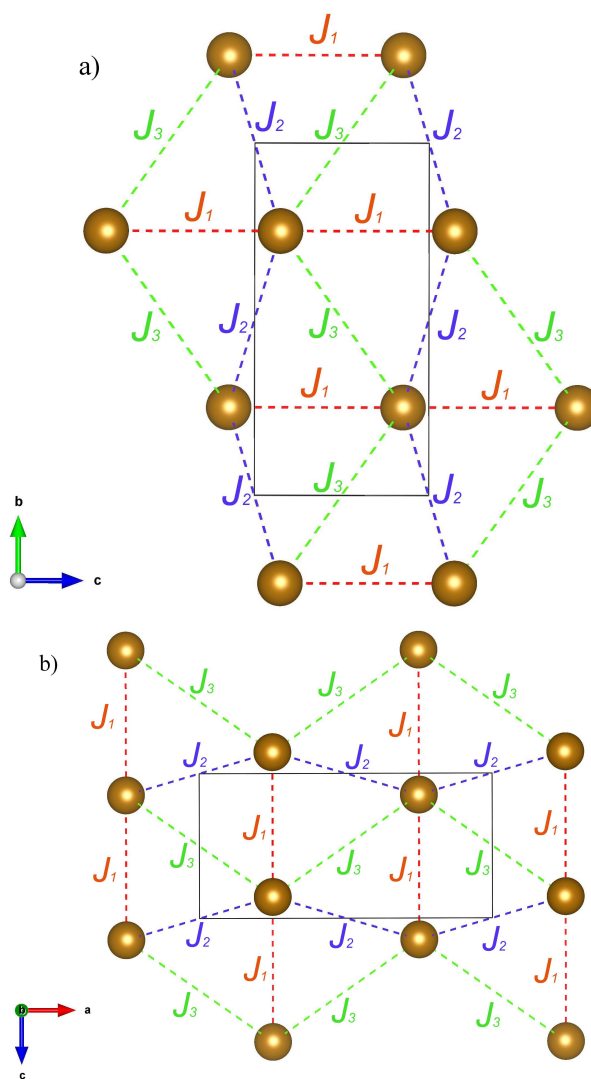


**Fig. 7** View along the  $a$ - and  $b$ -axis of the three magnetic interactions used to model the magnetic ground state below the ordering temperature. The  $J_1$ ,  $J_2$  and  $J_3$  exchange couplings have been represented in red, blue and green dashed lines, respectively. For clarity only the  $\text{Fe}^{3+}$  ions have been represented.

We can explore the possible magnetic structures (first ordered states) as a function of the relative values of the exchange interactions using the approach given in reference<sup>33</sup>. This method consists on the diagonalization of the Fourier transform of the exchange interaction matrix (functionally dependent on the  $\mathbf{k}$  vec-



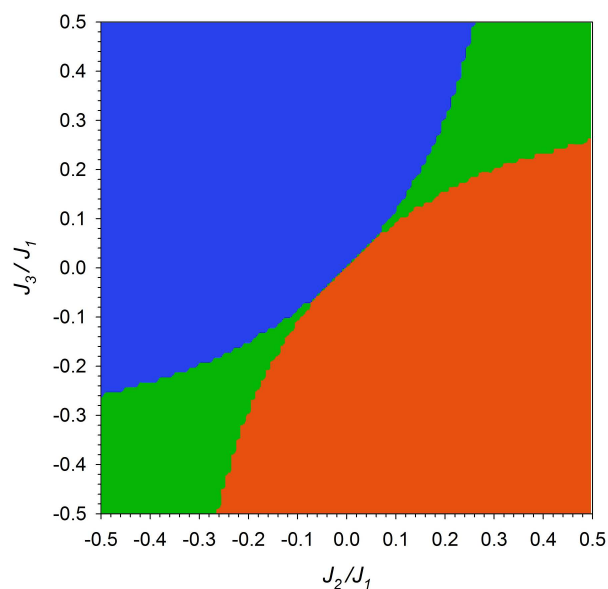


**Fig. 8** Magnetic phase diagram for  $J_1 = -18$  K. Phases colored as red and blue correspond to  $\mathbf{k} = (0, 0, \frac{1}{2})$  collinear antiferromagnetic magnetic structures, while the phase represented in green corresponds to disorder or incommensurate magnetic structures (see main text).

tor) and the exchange parameters. For the sake of simplicity, we assume that  $J_1 = -18$  K (as obtained from the magnetic susceptibility data) and  $\frac{J_2}{J_1}, \frac{J_3}{J_1}$  varying from -0.5 to +0.5. The complete phase diagram has been calculated using the programs SIMBO and EnerMag,<sup>34</sup> using the structural model derived from the low temperature Rietveld refinement. The Figure 8 shows the calculated phase diagram. This phase diagram represents a 2D map. Considering that  $J_1$  was fixed to -18, the  $J_2$ - $J_3$  interaction-space can be classified into three different regions. These regions correspond to different magnetic models. The region represented in blue color in Figure 8, corresponds to collinear antiferromagnetic structure with  $\mathbf{k} = (0, 0, \frac{1}{2})$  propagation vector and with magnetic moments of the two magnetic atoms in the primitive unit cell coupled as  $\Gamma_3$ . The second model corresponds to the region represented in red in Figure 8. This model presents the same propagation vector but follows the magnetic structure described by  $\Gamma_6$ . The last region groups all the situations in which no classical magnetic order exists or the magnetic structure is incommensurate due to competing interactions. Regarding the topology of the exchange coupling network, incommensurate structures due to frustration effects is the most plausible situation.

## 4 Conclusion

We have investigated the crystal structure of low dimensional fluoride  $\beta\text{-FeF}_3(\text{H}_2\text{O})_2\cdot\text{H}_2\text{O}$ , the structural studies have been carried out combining high-resolution powder X-ray and neutron diffraction. The high contrast of neutron diffraction allows us unambiguously to determine the H-atoms positions of both coordination and crystallization water molecules. On the other hand, we have confirmed the disordered model previously presented for the  $\text{F}^-$  ions and coordination water molecules. The extensive net-

work of H-bond present in  $\beta\text{-FeF}_3(\text{H}_2\text{O})_2\cdot\text{H}_2\text{O}$  compound could be the responsible for the long-range antiferromagnetic order observed at low temperature. From neutron diffraction, below  $T_N = 20(1)$  K,  $\beta\text{-FeF}_3(\text{H}_2\text{O})_2\cdot\text{H}_2\text{O}$  exhibits a long-range antiferromagnetic order commensurate with the lattice with  $\mathbf{k} = (0, 0, \frac{1}{2})$ . It is characterized by antiferromagnetic chains running along the  $c$ -axis which are coupled antiferromagnetically. Using mean-field approximation, we estimated the magnetic exchange-interaction parameters both between and within the chains. We found that  $J_{\parallel}/k_B = -18$  K and  $J_{\perp}/k_B = -3$  K in good agreement with the magnetic structure determined from neutron diffraction. Based on the possible exchange couplings obtained from the structural model we have created a magnetic phase diagram which reproduces the experimental results.

As other compositions within the  $\beta\text{-MF}_3\cdot 3\text{H}_2\text{O}$  ( $M = \text{V}, \text{Cr}, \text{Mn}, \text{Co}$ ) should be available, this family of materials related to the rosenbergite mineral would provide a playground to investigate the effect of the dimensionality of the spin on the magnetic ground state in this pseudo-1D family.

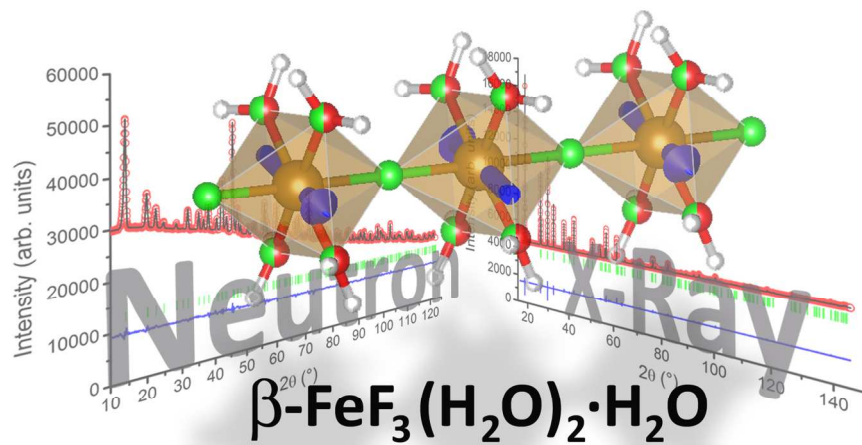
## Acknowledgments

The authors acknowledge the allocation of beamtime at the Institut Laue Langevin and the technical support provided during the experiment. G. Nénert thanks Thomas Witzke for bringing to his attention the existence of the rosenbergite mineral and Alexander van Lemel for technical support.

## References

- 1 P. Schiffer, *Nature* **413**, 48 (2001); R. Mossner, *Can. J. Phys.* **79**, 1283 (2001); R. Mossner and A. P. Ramirez, *Physics Today*, February 2006, p. 24; *Frustrated Spin Systems*, H. T. Diep, Ed. World Scientific Singapore, 2004. *Quantum Magnetism*, U. Schollwöck, *et al.*, Eds. (Lecture Notes in Physics 645) (Springer, Berlin 2004).
- 2 T. Masuda *et al.* *Phys. Rev. Lett.* **94**, 039706 (2005); S.-L. Drechsler *et al.* *Phys. Rev. Lett.* **98**, 077202 (2007).
- 3 L. Capogna, *et al.*; *Phys. Rev. B* **82**, 014407 (2010); L. Capogna, *et al.* *Phys. Rev. B* **71**, 140402(R) (2005).
- 4 G. Nénert, *et al.*, *Phys. Rev. B.* **82**, 024429 (2010); H. C. Hsu, H. L. Liu, F. C. Chou; *Phys. Rev. B* **78**, 212401 (2008); A. Ruydi, *et al.*; *App. Phys. Lett.* **92**, 262506 (2008).
- 5 Y. Naito, *et al.*; *J. Phys. Soc. Japan* **76** (2007) 023708; M. Enderle, *et al.*; *Europhys. Lett.* **70**, 237 (2005).
- 6 S. Furukawa, *et al.*; *Phys. Rev. Lett.* **105**, 257205 (2010).
- 7 G. Nénert, T. T. M. Palstra, *J. Phys.: Condens. Matter* **19** 406213 (2007); J. F. Scott, R. Blinc, *J. Phys.: Condens. Matter* **23** 113202 (2011); Y. Calage, W.M. Reiff, *J. of Solid State Chem.* **111**(2), 294-299 (1994); G. P. Gupta, D. P. E. Dickson, C. E. Johnson, B. M. Wanklyn, *J. Phys. C: Solid State Phys.* **11** 3889 (1978).
- 8 S. Sanghvi, N. Pereira, A. Halajko, G.G. Amatucci, *RSC Adv.* **4**, 57098- 57110, (2014); L. Liu; H. Guo, M. Zhou, Q. Wei, Z. Yang, H. Shu, X. Yang, J. Tan, Z. Yan, X. Wang, *Journal of Powder Sources*, **238**, 501- 515, (2013).
- 9 L. Li, Y. Yu, F. Meng, Y. Tan, R.J. Hamers, S. Jin, *Nano Lett.*

- 12, 724- 731, (2012).
- 10 F. Olmi, C. Sabelli, R. Trosti-Ferroni; *European Journal of Mineralogy* **5**, 1167-1174 (1993).
- 11 F. H. Herbststein, M. Kapon, G. M. Reisner, *Zeitschrift für kristallographie* **171**, 209-224 (1985).
- 12 W. F. Ehret, F. J. Frere, *J. Am. Chem. Soc.*, **67** 64-68 (1945); R. D. Freeman, *J. Phys. Chem.* **60**, 1152 (1956).
- 13 I. Dézsi, T. Pannaparayil, and L. N. Mulay, *Journal of Applied Physics* **61**, 4346 (1987).
- 14 Hansen T. C., Henry P. F., Fischer H. E., Torregrossa J., Convert P.; *Meas. Sci. Technol.* **2008**, 19 034001.
- 15 J. Rodríguez-Carvajal, *Physica. B*, **192**, 55 (1992). The programs of the FullProf Suite and their documentation can be obtained from Web at <http://www.ill.eu/sites/fullprof/>.
- 16 G. D. Gatta, G. Nénert, P. Vignola, *American Mineralogist*, Volume **98**, 1297-1301, (2013).
- 17 G. D. Gatta, P. Vignola, M. Meven, R. Rinaldi, *American Mineralogist*, **98**, 1624-1630, 2013.
- 18 O. Kahn, *Molecular Magnetism*, VCH: New York, 1993.
- 19 D. G. Karraker, P. K. Smith, *Inorg. Chem.* **31**, 1118-1120 (1992).
- 20 L. J. de Jongh and A. R. Miedema, *Adv. Phys.* **50**, 947 (2001).
- 21 H. J. Schulz, *Phys. Rev. Lett.* **77**, 2790 (1996).
- 22 *Magnetism and the chemical bond* by J. B. Goodenough, Interscience Publisher, Wiley and Sons, New York-London (1963).
- 23 M.E. Fisher, *Am. J. Phys.* **32**, 343 (1964).
- 24 H. Park, R. Lam, J.E. Greedan, J. Barbier, *Chem. Mater* **15**, 1703 (2003); Y. C. Arango, E. Vavilova, M. Abdel-Hafiez, O. Janson, A. A. Tsirlin, H. Rosner, S.-L. Drechsler, M. Weil, G. Nénert, R. Klingeler, O. Volkova, A. Vasiliev, V. Kataev, B. Büchner, *Phys. Rev. B* **84**, 134430 (2011).
- 25 J. Rodríguez-Carvajal, ILL-August 2007 k-Search program.
- 26 E. F. Bertaut, in *Magnetism*, edited by G. T. Rado and H. Shulz, (Academic, New York, 1963), Vol. III, Chap. 4.
- 27 J. Rodríguez-Carvajal, ILL-August 2007 BasIreps program.
- 28 H. T. Stokes, D. M. Hatch and J. S. Kim *Acta Cryst. A* **43**, 81-84 (1987).
- 29 H. T. Stokes, B. J. Campbell, and R. Cordes, *Acta Cryst. A* **69**, 388-395 (2013).
- 30 J.M. Perez-Mato, S.V. Gallego, E.S. Tasci, L. Elcoro, G. de la Flor, and M.I. Aroyo *Annu. Rev. Mater. Res.* (2015) doi:10.1146/annurev-matsci-070214-021008. The Bilbao Crystallographic Server and the program MAXMAGN are accessible at <http://www.cryst.ehu.es/>
- 31 K. M. Kojima, Y. Fudamoto, M. Larkin, G. M. Luke, J. Merriin, B. Nachumi, Y. J. Uemura, N. Motoyama, H. Eisaki, S. Uchida, K. Yamada, Y. Endoh, S. Hosoya, B. J. Sternlieb, and G. Shirane *Phys. Rev. Lett.* **78**, 1787 (1997).
- 32 P. Nunez, T. Roisnel, *J. Solid State Chem.* **124**, 338-345 (1996), P. Nunez, J. Darriet, P. Burkovec, A. Tressaud, P. Hagenmuller, *Mater. Res. Bull.* **22**, 661-667 (1987).
- 33 M. Freiser *J. Phys. Rev.* **123**, 2003, (1961).
- 34 N. El Khayati, R. Cherkaoui El Moursli, J. Rodríguez-Carvajal, G. André, N. Blanchard, F. Bourée, G. Collin, T. Roisnel, *Eur. J. Physics B* **22**(4), 429, (2001).



160x80mm (300 x 300 DPI)